

CHEMISTRY

A European Journal



Accepted Article

Title: Highest and Fastest Removal Rate of Pb(II) Ions through Rational Functionalized Decoration of a MOF Cavity

Authors: Farzaneh Afshariazar, Ali Morsali, Jun Wang, and Peter C. Junk

This manuscript has been accepted after peer review and appears as an Accepted Article online prior to editing, proofing, and formal publication of the final Version of Record (VoR). This work is currently citable by using the Digital Object Identifier (DOI) given below. The VoR will be published online in Early View as soon as possible and may be different to this Accepted Article as a result of editing. Readers should obtain the VoR from the journal website shown below when it is published to ensure accuracy of information. The authors are responsible for the content of this Accepted Article.

To be cited as: *Chem. Eur. J.* 10.1002/chem.201904436

Link to VoR: <http://dx.doi.org/10.1002/chem.201904436>

Supported by
ACES

WILEY-VCH

FULL PAPER

Highest and Fastest Removal Rate of Pb(II) Ions through Rational Functionalized Decoration of a MOF Cavity

Farzaneh Afshariazar^a, Ali Morsali^{a*}, Jun Wang^b and Peter C. Junk^b

^aDepartment of chemistry, Faculty of sciences, Tarbiat Modares University, Tehran, Iran

^bCollege of Science & Engineering, James Cook University, Townsville Old, 4811, Australia

Abstract: To overcome the challenge of developing a multipurpose adsorbent for effective removal of toxic and carcinogenic Pb (II) ions from aqueous solutions, a made-for-purpose functional group (N¹, N²-di(pyridine-4-yl)oxalamide) was rationally designed and incorporated into the cavities of a Zn-MOF, namely TMU-56. Large enough pore size along with high densities of strong metal chelating sites lead not only to the highest uptake capacity for Pb(II) ions, but also the fastest removal rate that has ever been reported for functionalized MOFs, occurred in just 20 sec. Moreover, high concentrations of lead ions favor the ion exchange reaction resulting in high degree of metal exchange. In addition, TMU-56 can be a practical adsorbent for its noticeable performance in simultaneous removal of several toxic and carcinogenic heavy metals from waste water which has rare precedence.

Introduction

Water contamination with heavy metal ions has led to an increasing global concern.^[1] Nowadays exponential growth of urbanization and industrial activities have led to high quantities of heavy metals discharge into water resources raising serious threats over their deleterious effect on environment and human health.^[2] Lead, one of the most toxic, prevalent and carcinogenic heavy metals, is highly non-degradable and tends to accumulate in the human body and induces severe damage to various human organs even at low concentrations.^[3] To date, various methods have been proposed and employed for removal of Pb(II) ions from wastewater.^[4] Among these various methods, adsorption is globally considered as one of the most desirable methods in water treatment due to its high adsorption capacity, simple design and cost efficiency.^[5] Despite all these advantages, extensive use of traditional adsorbents including zeolites,^[6] activated carbon,^[7] nanoparticle,^[8] and clays^[9] have been limited because of their low adsorption capacity, difficulties in recovery process and lack of proper functional groups to create strong binding

affinity/selectivity to metal centers. These inadequacies in water decontamination have led to considerable efforts to design and develop a novel generation of porous crystalline materials to achieve higher metal uptake capacity.

Metal-Organic Frameworks have been considered as unprecedented candidates for adsorptive removal of various heavy metals due to their unique properties including high surface areas, easily accessible cavities, and designable chemical functionalization of pore surfaces.^[10] The high potential of MOFs in water decontamination is related to their modular synthesis conditions by which strong adsorption sites can be purposefully introduced into the pore surfaces of MOFs through post-synthetic or pre-designing approaches to achieve high densities of chelating functional groups.^[11] Post-synthetic modification approaches have been widely used to incorporate proper active sites into MOFs to obtain increased adsorption capacities in Pb(II) removal. However, these post-modified materials do not display noticeable adsorption capacity for Pb(II) ions.^[12] In addition strong interactive sites with high binding affinity to heavy metal ions can be directly incorporated into MOFs through rationally pre-designed approaches.^[13] Regarding all these aspects, a judicious design and selection of proper functional groups will be a promising strategy in construction of functionalized MOFs to enhance contaminant removal from aqueous solutions. However, so far, there are few reports on pre-designed functionalized MOFs which have ideal functional groups to act as strong adsorption sites due to their low density and poor binding affinity for Pb(II) ions.

To overcome these challenges, we propose the development of a highly porous framework which possesses the following advantages: (i) large enough cavity size for facile diffusion of various contaminants into the framework; (ii) highly exposed pore surfaces decorated with specific chelating groups to achieve the best performance of host-guest interactions in the cavity of MOFs

FULL PAPER

for ultrahigh uptake capacity; (iii) multiple porosity heavily populated with well-distributed adsorption sites provides ultrafast removal of Pb(II) ions. To achieve these goals, we constructed a Zn(II)-MOF, TMU-56, densely decorated with oxamide functional groups which are directly exposed within MOF cavities. The oxamide motif (-NH-CO-CO-NH-) can be considered as a "double amide" which has been extensively studied for its high performance in gas adsorption applications.^[14] Dual functionalities which result from both CO- and NH- function sites in the oxamide motif, provide effective host-guest interactions in the MOF cavity. To the best of our knowledge, this is the first report of an oxamide-pillar based MOF which provides a proper coordination site to coordinate strongly and immediately to Pb(II) ions. Moreover, high concentrations of lead ions favor the ion exchange reaction resulting in high degree of metal exchange in the structure along with the ion sorption process results in ultrahigh removal capacity.

Experimental

Materials and Characterizations

All starting reagents and solvents used for synthesis were commercially available and used as received. Zinc nitrate hexahydrate, lead nitrate, ethylenediamine tetraacetic acid, Dichloromethane, N,N-Dimethylformamide, Oxalylchloride, 4-aminopyridine, and 4,4'-oxybisbenzoic acid were all purchased from Merck and Sigma-Aldrich.

Infrared spectra were recorded using Thermo Scientific Nicolet IR 100 FT-IR spectrometer. X-ray powder diffraction (XRD) measurements were done by a Philips X'pert diffractometer with mono chromated Cu-K α radiation. Thermal curves were obtained on a PL-STA 1500 apparatus with the heating rate of 10°C /min up to 800 °C under a constant flow of nitrogen. NMR spectrum was obtained on a Bruker AC-500 MHz NMR spectrometer. SEM and EDS analysis were performed by TESCAN MIRA instrument. Residual concentration of metal ions were determined by simultaneous inductively coupled plasma optical emission spectrometry (ICP-OES) on a Varian Vista-PRO instrument (Springvale, Australia) using a charge-coupled detector. X-ray photoelectron spectroscopy (XPS) was also conducted with a Thermo Scientific, ESCALAB 250Xi Mg X-ray resource. N₂ adsorption-desorption investigation was performed at 77° K by using Micromeritics Instrument Corporation (TriStar II).

Synthesis of N¹, N²-di(pyridine-4-yl)oxalamide ligand (ox)

To a solution of 4-aminopyridine (2.35 g, 25 mmol) in 100 mL CH₂Cl₂ at 273°K, was added 5 mL triethylamine and the mixture

was stirred for 10 min. A solution of oxalyl chloride (1.1 mL, 12.5 mmol) in 20 mL CH₂Cl₂ was added dropwise to the reaction mixture over 3 h at 273°K. The reaction mixture was then stirred for an additional 12 h at room temperature and then the solvent was removed under vacuum. The precipitate was filtered, washed 3 times with 100 mL distilled water and then dried at room temperature. Yield: 75%. FT-IR data (KBr pellet, cm⁻¹) selected bands: 3279-2983 (vs), 1693 (s), 1588 (vs), 1501 (vs), 1401 (m), 1329 (s), 1277 (s), 1212 (s), 1152 (m), 991 (m), 866(m), 823 (m), 693 (m), 523 (m), 487 (m). ¹H-NMR (500 MHz, [d₆] DMSO, 25°C): δ = 11.28 (s, 2H; NH), 8.53-8.54 (d, 4H; CH₂), 7.87-7.88 (d, 4H; CH₂).

Synthesis of TMU-56

Single crystals of TMU-56 were prepared by the following procedure: Zn(NO₃)₂·6H₂O (0.297 g, 1 mmol), N¹, N²-di(pyridine-4-yl)oxalamide ligand (0.121 g, 0.5 mmol) and 4,4'-oxybisbenzoic acid (0.258 g, 1 mmol) were dissolved in 15 mL DMF. The reaction mixture was then heated in a pre-heated oven at 80°C in glass vials. Colorless crystals were obtained after 72 h. FT-IR data (KBr pellet, cm⁻¹) selected bands: 3429 (vs), 1704 (m), 1669 (m), 1607 (s), 1500 (m), 1416 (s), 1242 (s), 1157 (m), 874 (m), 778 (m), 548 (m).

Sorption study

Pb(II) stock solution with the concentration of 1000 ppm was prepared by dissolving Pb(NO₃)₂ salt in distilled water. Other Pb(II) solutions with various concentration were prepared by diluting the appropriate amount of the stock solution. In all sorption experiments 5 mg of TMU-56 was applied as a solid adsorbent and the adsorption experiments were performed at room temperature. Subsequently, the residual metal content was measured by using ICP-OES spectrometer.

pH study

To investigate the influence of pH as a key factor on Pb(II) removal, adsorption experiments were carried out on various sample solutions with initial pH value ranging from 3 to 8. Adjustment of pH was carried out on 100 ppm Pb(II) solution by adding either 0.1M NaOH or 0.1M HCl solutions. Surface charge of TMU-56 was also measured at different pH values for further investigation. Considering all these results, pH=7 was selected as an optimum pH value for subsequent uptake experiments (Figures S22, S23). It should be also mentioned that the decomposition of TMU-56 occurred below pH value of 3 and the precipitation of Pb(II) ions happened above pH=8. The equilibrium

FULL PAPER

Pb(II) uptake capacity, Q_e (mg/g), was determined by Equation A. 1

$$Q_e = \frac{(C_0 - C_e)V}{m} \quad (\text{A. 1})$$

Where C_0 and C_e are the initial and equilibrium Pb(II) concentrations (mgL^{-1}), respectively. V (L) is the volume of solution and m (g) is the adsorbent mass.

Adsorption kinetics study

5 mg of TMU-56 was added into a glass beaker containing 25 mL of 50 ppm Pb(II) solution. At different times (10 sec to 120 min), the adsorption process was stopped and sampling was done. Then, the mixture was filtered through a 0.22 μm membrane filter and the filtrate was applied for determining the residual concentration of Pb(II) ions by ICP-OES spectrometer.

Pb²⁺ adsorbed quantities were calculated using Equation A. 2:

$$Q_t = \frac{(C_0 - C_t)V}{m} \quad (\text{A. 2})$$

Where Q_t (mgg^{-1}) is the total amount of Pb(II) ions adsorbed at time t (min), C_0 and C_t are the initial and equilibrium Pb(II) concentrations (mgL^{-1}) at time t (min), respectively. V (L) is the volume of solution and m (g) is the adsorbent mass.

Adsorption isotherm study

To study the adsorption isotherm, 5 mg of TMU-56 was added to 25 mL of Pb(II) solution with different initial concentrations varying from 20 to 280 ppm and stirred for 1 h at room temperature. Then, the mixture was centrifuged at 14000 rpm for 5 min, and the remaining concentration of Pb(II) was determined via ICP. The equilibrium Pb(II) uptake capacity, Q_e (mgg^{-1}), was determined by Equation A. 1.

The Langmuir isotherm model was used to estimate the adsorption model of Pb(II) ions on TMU-56 by simulating the equilibrium adsorption data. The Langmuir isotherm model can be expressed as Equation A. 3:

$$\frac{C_e}{q_e} = \frac{C_e}{q_m} + \frac{1}{q_m K_L} \quad (\text{A. 3})$$

Where q_m (mgg^{-1}) is the maximum adsorption amount of Pb(II) on TMU-56, and K_L is the Langmuir constant.

Cycle performance study.

For desorption studies, a low concentration solution of Pb²⁺ ions was applied. 5 mg of adsorbent was added to a 25 mL solution of 10 mgL^{-1} of Pb(II) ions. The desorption process was carried out by adding 10 mL of 0.1 M of EDTA.2Na solution to the solid adsorbent and the solution was then stirred for 10 min at room temperature. The amount of desorbed Pb(II) ions was determined with ICP-OES.

Results and discussion

Structural analysis of TMU-56

$[\text{Zn}_2(\text{ox})(\text{oba})_2] \cdot 2\text{DMF}$, TMU-56, crystallizes in the monoclinic $P2_1/c$ space group. TMU-56, consists of a binuclear Zn_2 carboxylate unit (Zn#1 and Zn#2), in which both Zn(II) metal centers can be considered as distorted tetrahedral units that coordinate to three fully deprotonated tetrahedral units that coordinate to three fully deprotonated dicarboxylate (oba⁻) ligands (for Zn#1: O1, O5, O10, and for Zn#2: O4, O6, O9) and one nitrogen atom (Zn#1: N1 and Zn#2: N4) from the N¹, N²-di(pyridine-4-yl)oxalamide ligand (Figure 1a). The distance between two adjacent metal centers (Zn#1 and Zn#2) is 3.363 Å. H_2oba acts as a nonlinear dicarboxylate ligand and coordinates to three successive metal centers from two various dinuclear Zn_2 units, resulting in the formation of 2D sheets. Two carboxylate groups in the H_2oba ligand exhibit diverse coordination modes: one of the carboxylate groups acts as a bidentate chelating group and bridges between two Zn#1 and Zn#2 centers of the binuclear cluster unit in a *syn-syn* mode, while the other one acts as a monodentate ligand and coordinates to either Zn#1 or Zn#2 metal centers. Zinc-carboxylate layers are successfully extended through bipyridyl-based pillars to form 3D crystalline framework (Figure 1b). Despite the formation of double interpenetration in TMU-56, large 1D honeycomb-like channels of approximately 16×4.77 Å (including van der Waals radii) occur in the $[1\ 0\ 1]$ direction which are densely decorated with oxamide groups pointing into the pores (Figures 1c, 1d).

Characterization of TMU-56

The phase purity of as-synthesized TMU-56 was confirmed by a PXRD pattern which was in good agreement with the simulated one (Figure S1). Thermogravimetric analysis (TGA) indicates a gradual weight loss of 14.9% up to 220 °C, which corresponds to the removal of DMF solvent molecules. This framework displays thermal stability up to 370 °C, afterwards a distinctive weight loss occurs in the range of 370-580 °C suggesting a disintegration of the host net (Figure S2). The activation process for adsorption studies was successfully performed by solvent exchange with acetonitrile for 5 days. PXRD analysis reveals that the crystallinity of the structure remains intact after activation process (Figure S3). The permanent porosity of TMU-56 was evaluated by N_2 -gas

FULL PAPER

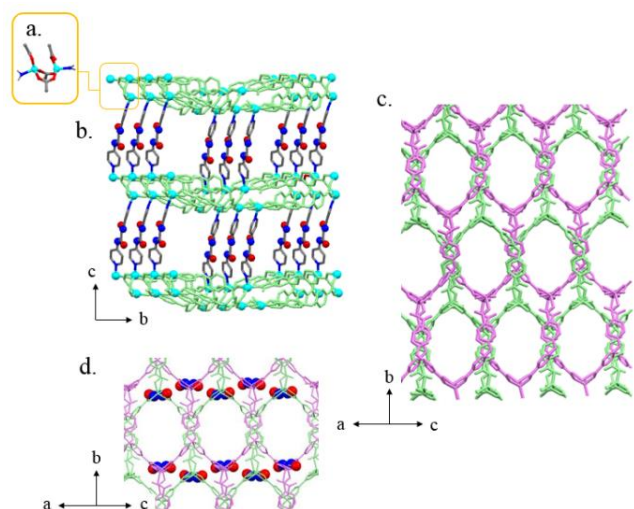


Figure 1. (a) Ball and stick representation of binuclear Zn_2 unit (color code: Zn: cyan; O: red; N: blue; C: gray). (b) 2D-layers of Zn(II)-oba unit pillared by the oxamide ligand. (c) A view of doubly interpenetrated framework possessing 1D honey-comb pores along $[1\ 0\ 1]$ direction. (d) Representation of honey-comb pores highlighting the oxamide group containing CO- and NH- function groups pointing toward the pores of TMU-56.

adsorption studies at 77 K and 1 bar. BET surface area based on nitrogen adsorption isotherms was calculated to be $650\text{ m}^2/\text{g}$. A very sharp uptake occurred at $P/P_0 < 0.05$ consistent with a type-I isotherm characteristic of a microporous structure (Figure S4).^[15]

Adsorption studies

Uptake capacity and adsorption kinetics are two of the most important key factors for performance assessment of a practical adsorbent. Moreover, the pH value is considered as one of the most important factors in Pb(II) adsorption from aqueous solutions. It is believed that the pH of the solution determines the availability of the various species of the Pb(II) ions in solution, the surface charge of the adsorbent, as well as the ionization degree of the functional groups which are on the surface of the adsorbent. In low pH, the dominant species in the solution are Pb^{2+} ions, whereas by exceeding the pH value, $Pb(OH)^+$ ions are considered as the dominant species at $pH=7.5$, which ultimately results in the precipitation of $Pb(OH)_2$.^[16] The effect of pH on the adsorption of Pb(II) by TMU-56 was studied in the pH range of 3-8. As illustrated in Figure S23, TMU-56 has the most negative surface charge at $pH=7$ which might be considered as a driving force for Pb(II) adsorption resulting in high capture of Pb(II) ions at $pH=7$. Moreover, after adding TMU-56 to Pb(II) solution, the pH value of the solution was remeasured which had been reached to $pH=6$.

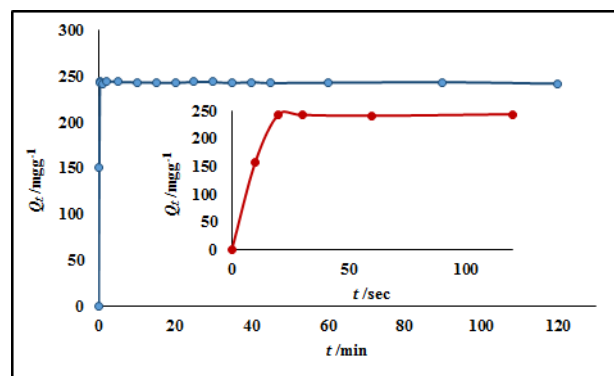


Figure 2. Effect of various contact time on Pb(II) adsorption by applying 5 mg TMU-56 with initial concentration of 50 ppm; Q_t : the amount of Pb(II) adsorbed on TMU-56 at different times.

Pb(II) removal rates were investigated by using 5 mg TMU-56 in 50 ppm Pb(II) solution at an optimum pH value of 7.0 at various time intervals (10 sec to 120 min).

Extraordinarily, over 97% of Pb(II) removal was achieved in just 20 seconds (Figure 2). To the best of our knowledge, this is the most rapid, record-breaking time that has ever been reported for functionalized MOFs in water decontamination, which can be attributed to inherent properties of TMU-56 arising from large enough pore size and densely cavity decoration with strong chelating sites. A pseudo-second-order kinetic model with maximum correlation coefficient ($R^2=0.9998$) was applied to fit the experimental kinetic results (Equation A. 4), suggesting that the rate controlling step for Pb(II) adsorption onto TMU-56 is predominantly chemical (Figure 3).^[17]

$$\frac{t}{q_t} = \frac{1}{k_2 q_e^2} + \frac{t}{q_e} \quad (\text{A. 4})$$

where k_2 ($\text{g mg}^{-1} \text{min}^{-1}$) points to the pseudo-second-order rate constant, q_t (mg g^{-1}) is the total amount of Pb(II) ions adsorbed at time t (min), and q_e (mg g^{-1}) is the maximum amount of Pb(II) adsorbed at equilibrium.

To investigate the uptake capacity of TMU-56 in Pb(II) removal, different concentrations of Pb(II) solutions ranging from 20-280 ppm were applied. As illustrated in Figure 4, by increasing the initial concentration of Pb(II) solutions, a rapid increase in adsorption of Pb(II) ions on TMU-56 was observed, which indicates that the adsorbent (TMU-56) has a strong affinity for adsorbate (Pb(II) ions) which can be ascribed to the abundant metal chelating groups within the MOF cavities.

FULL PAPER

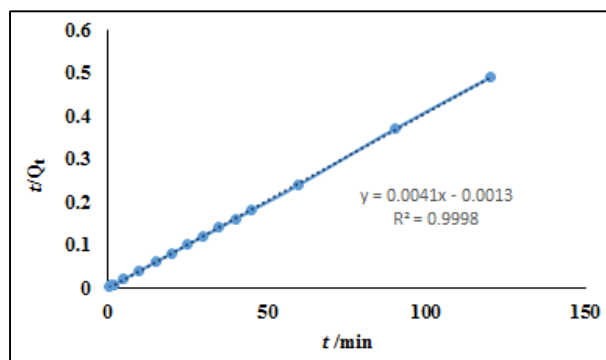


Figure 3. Pseudo-second-order kinetics model of Pb(II) adsorption on TMU-56.

It should be also mentioned that at high concentrations of lead ions ion exchange reaction occurred along with the ion sorption process resulting in ultrahigh removal capacity.

Moreover the experimental adsorption data were well fitted with the Langmuir isotherm, signifying a monolayer-type adsorption (Figure 4).^[18]

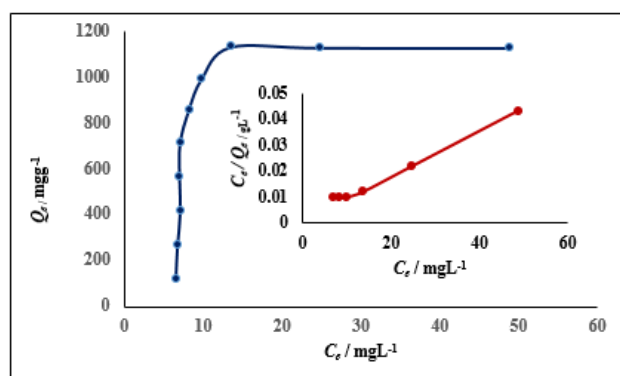


Figure 4. Adsorption isotherm of TMU-56 for Pb(II) ions. Inset displays linear regressions by fitting equilibrium adsorption data with Langmuir isotherm.

A remarkable saturation adsorption capacity of 1130 mg Pb/gr TMU-56, which was attained at equilibrium, is a record-breaking uptake capacity among all MOF-based adsorbent materials achieved so far (Table 1). The oxamide motif (-NH-CO-CO-NH-) with "back to back" amide functional groups is responsible for unprecedented properties of TMU-56 in Pb(II) removal, in comparison to previously reported structures which contain separate amide groups in their structures (Figure S5).^[13b] Thermodynamic studies were carried out at 298-328 K to understand the nature of the Pb(II) adsorption process. Thermodynamic parameters for Pb(II) adsorption on TMU-56 are presented in Table S3. Thermodynamic parameters were calculated based on the following Equations:

Table 1. Comparison of Pb(II) adsorption by various MOFs.

MOF	Q_m (mg g^{-1})	Adsorption time (min)	pH	Ref.
Dy(BTC)(H ₂ O)(DMF) _{1.1}	5.073	10	6.5	25
MIL-101	15.78	30	6	26
{[Cd(ADB)L ₂]-1.5DMF-2H ₂ O} _n	63.052	6	7	13c
O-TMU-40	217	>10	7	27
TMU-4	237	15	10	11e
TMU-5	251	15	10	11e
TMU-6	224	15	10	11e
TMU-21	221	10	8	13b
TMU-23	267	10	8	13b
TMU-24	256	10	8	13b
[Zn ₃ L ₃ (BPE) _{1.5}] _n .4.5DMF	616.6	7	6	13d
MOF-5	659	30	5	28
MnO ₂ -MOF	917	60	5	29
TMU-56	1130	20 sec	7	This work

$$K_0 = \frac{Q_e}{C_e} \quad (\text{A. 5})$$

$$\Delta G^\circ = -RT \ln K_0 \quad (\text{A. 6})$$

$$\ln K_0 = \frac{\Delta S^\circ}{R} - \frac{\Delta H^\circ}{RT} \quad (\text{A. 7})$$

Negative values of ΔH and ΔG confirmed that the adsorption process is exothermic and spontaneous. In addition a positive value of ΔS indicates the irregularity enhancement at the solid-liquid interface during the Pb(II) adsorption (Figure S6).^[19]

Simultaneous decontamination of various heavy metal ions from waste water is of urgent need. Most of the traditional adsorbents show a moderate affinity to one or two kinds of heavy metals, while high concentrations of other heavy metals remain intact. To estimate the selectivity towards various heavy metals, a mixed solution containing 25 $\text{mg} \cdot \text{L}^{-1}$ of each heavy metal ions (Pb^{2+} , Hg^{2+} , Cr^{3+} , Cu^{2+} , Co^{2+} , and Cd^{2+}) in 25 mL aqueous solution was used. The results are illustrated in Figure S7 and demonstrate high capture performance of TMU-56 towards toxic and carcinogenic heavy metals with removal efficiency over 99%. This exceptional performance can be attributed to the rational functionalized decoration of the MOF cavity, resulting in strong host-guest interactions, which can make it as a practical adsorbent for

FULL PAPER

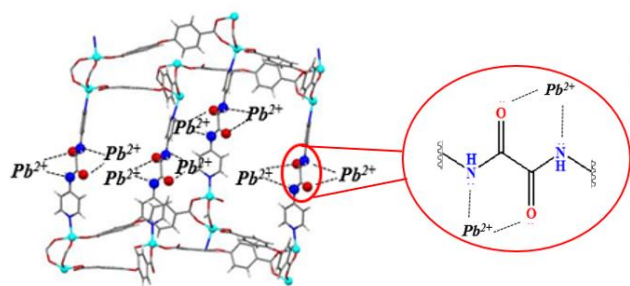


Figure 5. Schematic representation of Pb(II) chelation to oxamide motif.

multiple metal-scavenging. As-synthesized TMU-56 was immersed in water for 48 h to evaluate the chemical stability. Stability in water is a key factor in water decontamination. Further studies were conducted by PXRD analyses demonstrating the high chemical stability of the structure after prolonged immersion in water (Figure S8). To evaluate the reusability of TMU-56, two successive adsorption-desorption cycles were performed. Based on the MOFs Structures and the metal nodes, various methods can be applied for regeneration process. Acidic or alkaline media are suitable for this purpose. However, because of the strong interaction which exists between some of the host-guest species or the low stability of the structure in the acidic medium, EDTA solution with high affinity to various metal centers even in neutral conditions is desired. Pb-EDTA is soluble in the solution and by simple filtration through a 0.22 μm membrane filter, the desorbed MOF is separated and the filtrate is measured by using ICP-OES to determine the concentration of Pb^{2+} ions. As illustrated in Figure S9, acceptable adsorption-desorption yields were obtained. PXRD analysis was also conducted to evaluate the stability of the structure after desorption process. As shown in Figure S10, the crystallinity of the structure is preserved. It is obvious that the existence of abundant strong chelating sites within the pores can be result in strong chelation to metal ions (Figure 5).

Adsorption mechanism

TMU-56 was obtained under solvothermal conditions as microcrystalline powder. Several attempts were done to achieve larger single crystals to evaluate their performance in Pb(II) adsorption based on single crystal X-ray measurements. Unfortunately, the attempts were not successful and larger single crystals did not obtain. Moreover, after the sorption process the microcrystals didn't have good enough quality to perform the single crystal analysis on them.^[20]

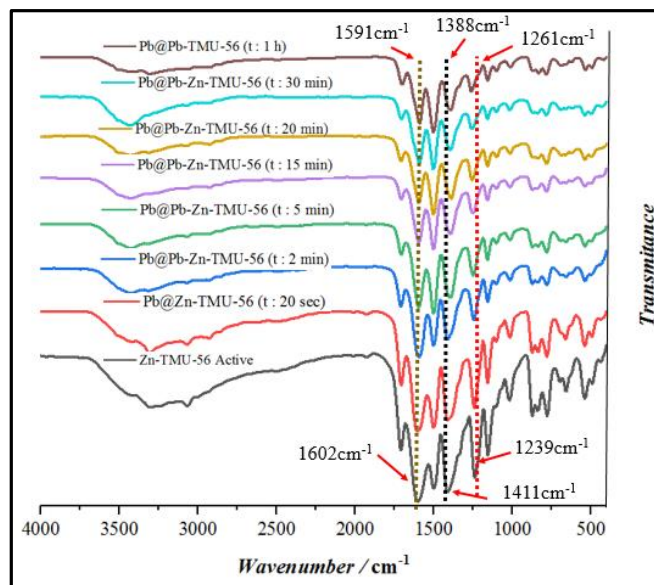


Figure 6. IR spectrum of TMU-56, before and after Pb(II) adsorption at various time intervals.

In order to investigate the probable adsorption mechanism, extended characterization techniques including Infrared spectroscopy, PXRD experiments and X-ray photoelectron spectroscopy were conducted. To examine the step-by-step mechanism of Pb(II) adsorption within the MOF pores, a solution with a specific concentration of Pb(II) ions (75 mgL^{-1}) was selected and sampling was done at various time intervals (20 sec to 60 min). After Pb(II) ions sorption, a new peak at 625 cm^{-1} was observed in IR spectrum, which can be assigned to Pb-O stretching vibration (Figure S11).^[21] As illustrated in Figure 6, the chelation is the major phenomenon at the initial stages of Pb(II) adsorption. Strong chelation of Pb(II) ions by the oxamide group reveals an obvious shift of C-N vibration mode in oxamide motif from 1239 cm^{-1} to 1261 cm^{-1} by increasing the contact time from 20 sec to 60 min.^[22] Moreover, when the sorption process proceeds, two other obvious shifts can be recognized in the IR spectrum. These distinct chemical shifts can be attributed to the symmetric and asymmetric vibration modes of the coordinated carboxylate groups to the metal centers which have been shifted to lower frequencies upon Pb(II) adsorption within the framework (Figure 6 and Table S4). This observation is indicative of a new event which occurs during the sorption process. This phenomenon can be attributed to the ion exchange reaction taken place between Pb(II) and Zn(II) ions. The metal exchange reaction is a well-known phenomenon in MOFs due to the various factors such as binding strength of metal-ligands or coordinative

FULL PAPER

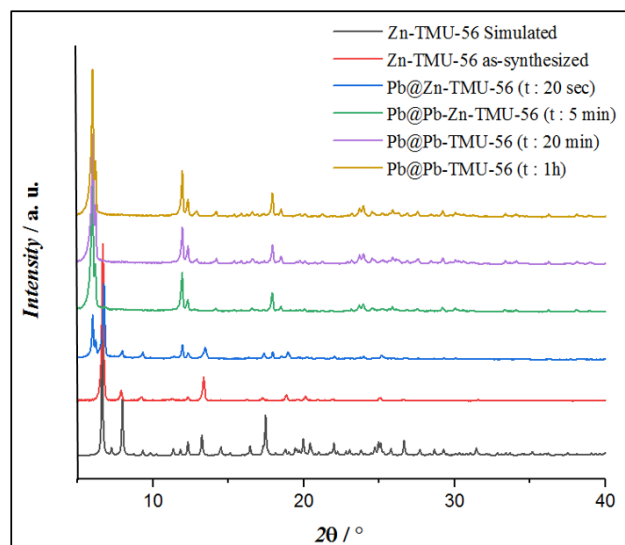
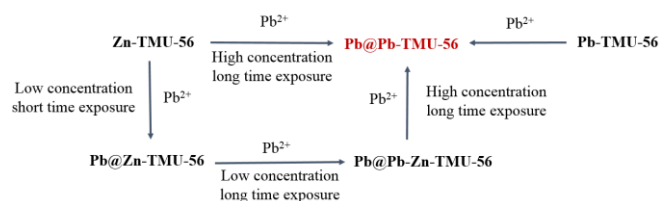


Figure 7. PXRD patterns of **TMU-56** after **Pb(II)** adsorption at various time intervals.

flexibility of the ligands in the framework.^[23] **Pb(II)** ions have greater coordination ability towards carboxylate groups in comparison to **Zn(II)** ions, so that the **Zn(II)** metal centers in the framework can be easily attacked and replaced by **Pb(II)** ions. High concentrations of lead ions favor the ion exchange reaction resulting in high degree of metal exchange. To verify this hypothesis a set of sorption experiments were conducted on a 75 mgL⁻¹ solution of **Pb(II)** ions at different time intervals and the residual metal content was determined using ICP-OES. As illustrated in Figure S12, **Pb(II)** ions concentration decreases sharply in a matter of seconds and then it becomes stable, while the concentration of **Zn(II)** ions is gradually increased after 2 min and then tends to be stable after 10 min. It can be concluded from these observations that the chelation mechanism is the predominant process at the initial stages of the adsorption process, followed by the metal exchange reactions resulting in the departure of **Zn(II)** metal ions from the framework, as well as providing a record-breaking removal rate and high uptake capacity of **Pb(II)** ions.

The effect of **Pb(II)** adsorption on the hosting framework of **TMU-56** was also analyzed by PXRD experiments. In order to compare all the results more precisely, the same experimental conditions (75 mgL⁻¹ solution of **Pb(II)** ions and different time intervals (20 sec to 60 min) were chosen. The PXRD patterns are given in Figure 7. It is apparent that at the initial stages of adsorption process (contact time: 20 sec) a structural transformation is appeared which indicates the formation of a new phase in the



Scheme 1. Schematic representation of **Pb(II)** adsorption on **TMU-56** at different time exposure and concentration of **Pb(II)** ions.

structure. By proceeding the adsorption process the peak with 2θ of about 7.9° is completely disappeared and new peaks with 2θ of about 11.9° , 17.9° , and 24.1° are appeared which are indicative of structural transformations in the framework.

For further investigation on **Pb(II)** adsorption mechanism, a **Pb-MOF** was synthesized by direct reaction of **Pb(CH₃COO)₂**, oxamide and Oba ligands (1:0.5:1), namely **Pb-TMU-56**. This **Pb-MOF** was applied to adsorb **Pb(II)** ions from a 100 mgL⁻¹ **Pb(II)** solution. Similar pattern was observed in the PXRD patterns of **Zn-TMU-56** and **Pb-TMU-56** after **Pb(II)** removal (Figure S13). The characteristic structural transformations were also occurred in PXRD patterns of **Pb-TMU-56** after **Pb(II)** removal (**Pb@Pb-TMU-56**) which reveals that this structural transformation might be attributed to the chelation of **Pb(II)** ions to the oxamide motif (Figure 5). A schematic representation of the effect of time exposure and concentration of **Pb(II)** ions on **Zn-TMU-56** and **Pb-TMU-56** is illustrated in scheme 1. XPS analysis was also performed to provide more information on the sorption mechanism. Low and high concentrations of **Pb(II)** ions were chosen for these measurements. As illustrated in Figure 8, after **Pb(II)** adsorption new peaks have been appeared in the XPS spectrum which can be attributed to the **Pb 4f**, **Pb 4d** and **Pb 4p**. In the high resolution spectrum of **Pb 4f** (Figure S14), the energy separation of about 5 eV between the **Pb 4f_{5/2}** and **Pb 4f_{7/2}** peaks (4.9 eV for low concentration of **Pb(II)** ions and 5.16 eV for high concentration of **Pb(II)** ions) can be attributed to **PbO**, suggesting that **Pb(II)** has been bonded with the O atoms within the framework.^[13c, 24] Upon **Pb(II)** loading, the core level of **N1s** is shifted to much higher binding energy (401.04 eV and 401.87 eV for low and high concentration of **Pb(II)** ions, respectively) in comparison to as-synthesized **TMU-56** (400.28 eV), which is indicative of the valance change of N atom in the oxamide motif due to the interaction with the **Pb(II)** ions (Figure S15)^[22] In addition, as illustrated in the high resolution XPS spectra (Figures S16 and S17), after adsorption of **Pb(II)** ions, the peaks of **O1s**

FULL PAPER

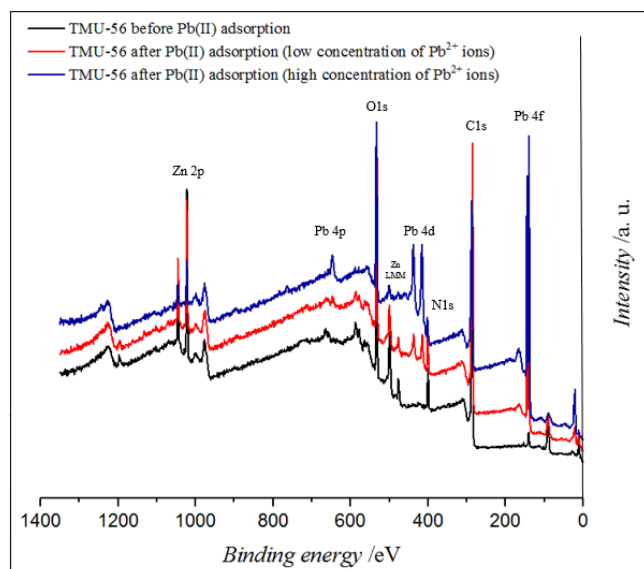


Figure 8. Wide-scan XPS spectra of **TMU-56**, before and after Pb(II) adsorption.

and C1s are all shifted to higher binding energies, suggesting the formation of Pb-O or Pb-OC bonding within the framework.^[24]

As shown in Figure 8, after loading a high concentration of Pb(II) ions, the relative intensity of Zn 2p peaks is reduced due to the metal exchange reaction between Zn(II) and Pb(II) ions and departure of Zn(II) from the framework (Figure S18). All these observations might lead to this conclusion that the oxamide motif is the major factor for high and fast uptake of Pb(II) ions from aqueous solutions. Also it can be proposed that due to the main role of the oxamide motif in chelation to the metal centers, it may be also act as an intermediate to facilitate the metal exchange process during the sorption process.

Further investigation was performed by EDX and SEM analysis before and after Pb(II) adsorption (Figure S19). Elemental mapping of Pb-loaded TMU-56 demonstrates the presence of densely adsorbed Pb(II) ions in the framework (Figure S20). No obvious change was observed in surface morphology of TMU-56, confirming that the crystals did not collapse during the loading process (Figure S21).^[13d]

Conclusions

In conclusion, remarkable results were attained in this work including the highest and fastest Pb(II) removal through rational decoration of the MOF cavity by a pre-designed N-donor ligand (ox). Incorporating this unprecedented motif to the pore walls of TMU-56 along with ion exchange reaction give rise not only to the

highest uptake capacity for Pb(II) ions of 1130 mgg⁻¹, but also exhibits a record-breaking time that has ever been reported for Pb²⁺ removal rate and results in high removal efficiency > 97% in just 20 sec. In addition various toxic and carcinogenic metals can be adsorbed efficiently from aqueous solutions due to the strong coordination affinity of the oxamide group to metal centers. Construction of TMU-56 by considering important key factors such as abundant metal chelating sites, high porosity, large enough cavity size and a proper geometry of coordination sites resulted in the formation of an effective and practical adsorbent. Our future goal is focused on designing other relevant functional groups to construct novel MOFs and examine their potential function in diverse fields.

Acknowledgments

This work was supported by Tarbiat Modares University.

Keywords: Adsorption. Metal-organic frameworks. Pb(II) ions. Wastewater.

References

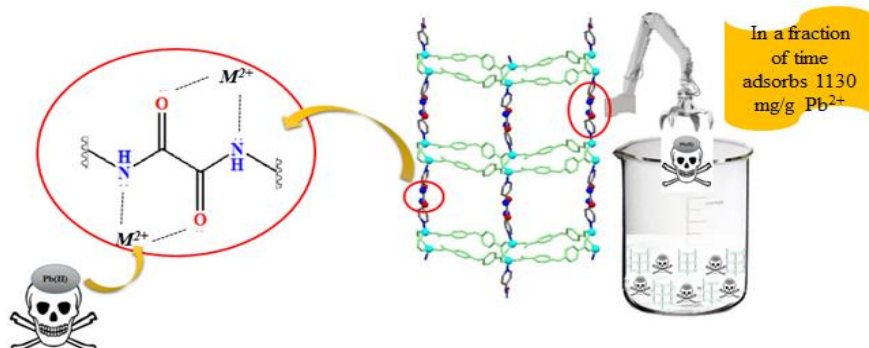
- [1] C. J. Vörösmarty, P. B. McIntyre, M. O. Gessner, D. Dudgeon, A. Prusevich, P. Green, S. Glidden, S. E. Bunn, C. A. Sullivan, C. Reidy Liermann, P. M. Davies, *Nature* **2010**, *467*, 555–561.
- [2] P. B. Tchounwou, C. G. Yedjou, A. K. Patlolla, D. J. Sutton, *EXS* **2012**, *101*, 133–164.
- [3] a) E. G. Moreira, I. Vassilieff, V. S. Vassilieff, *Neurotoxicol Teratol* **2001**, *23*, 489–495; b) X. Luo, L. Liu, F. Deng, S. Luo, *J. Mater. Chem. A* **2013**, *1*, 8280–8286; c) M. A. Assi, M. N. M. Hezme, A. W. Haron, M. Y. M. Sabri, M. A. Rajion, *Vet World* **2016**, *9*, 660–671; d) H. Hu, R. Shih, S. Rothenberg, B. S. Schwartz, *Environ. Health Perspect.* **2007**, *115*, 455–462.
- [4] F. Fu, Q. Wang, *J. Environ. Manage.* **2011**, *92*, 407–418.
- [5] a) I. Ali, *Chem. Rev.* **2012**, *112*, 5073–5091; b) D. Vilela, J. Parmar, Y. Zeng, Y. Zhao, S. Sánchez, *Nano Lett.* **2016**, *16*, 2860–2866.
- [6] X. Lu, F. Wang, X. Li, K. Shih, E. Y. Zeng, *Ind. Eng. Chem. Res.* **2016**, *55*, 8767–8773.
- [7] D. Kolodynska, J. Krukowska, P. Thomas, *Chem. Eng. J.* **2017**, *307*, 353–363.
- [8] Y. Bagbi, A. Sarswat, D. Mohan, A. Pandey, P. R. Solanki, *Sci. Rep.* **2017**, *7*, 7672.
- [9] J. U. K. Oubagaranadin, Z. V. P. Murthy, *Ind. Eng. Chem. Res.* **2009**, *48*, 10627–10636.
- [10] a) S. Rapti, A. Pournara, D. Sarma, I. T. Papadas, G. S. Armatas, Y. S. Hassan, M. H. Alkordi, M. G. Kanatzidis, M. J. Manos, *Inorg. Chem. Front.* **2016**, *3*, 635–644; b) S. Rapti, D. Sarma, S. A. Diamantis, E. Skliri, G. S. Armatas, A. C. Tsipis, Y. S. Hassan, M. Alkordi, C. D. Malliakas, M. G. Kanatzidis, T. Lazarides, J. C. Plakatouras, M. J. Manos, *J. Mater. Chem. A* **2017**, *5*, 14707–14719; c) P. A. Kobielska, A. J. Howarth, O. K. Farha, S. Nayak, *Coord. Chem.*

FULL PAPER

- Rev. **2018**, *358*, 92–107; d) J. E. Efome, D. Rana, T. Matsuura, C. Q. Lan, *ACS Appl. Mater. Interfaces* **2018**, *10*, 18619–18629.
- [11] a) F. Ke, L.-G. Qiu, Y.-P. Yuan, F.-M. Peng, X. Jiang, A.-J. Xie, Y.-H. Shen, J.-F. Zhu, *J. Hazard. Mater.* **2011**, *196*, 36-43; b) M. Carboni, C. W. Abney, S. Liu, W. Lin, *Chem. Sci.* **2013**, *4*, 2396-2402; c) L. Liang, Q. Chen, F. Jiang, D. Yuan, J. Qian, G. Lv, H. Xue, L. Liu, H. Jiang, M. Hong, *J. Mater. Chem. A* **2016**, *4*, 15370–15374; d) L. Aboutorabi, A. Morsali, E. Tahmasebi, O. Büyükgüngör, *Inorg. Chem.* **2016**, *55*, 5507–5513. e) E. Tahmasebi, M. Y. Masoomi, Y. Yamini, A. Morsali, *Inorg. Chem.* **2015**, *54*, 425-433.
- [12] a) D. T. Sun, L. Peng, W. S. Reeder, S. M. Moosavi, D. Tiana, D. K. Britt, E. Oveisi, W. L. Queen, *ACS Cent. Sci.* **2018**, *4*, 349-356; b) X. Luo, L. Ding, J. Luo, *J. Chem. Eng. Data* **2015**, *60*, 1732–1743; c) H. Saleem, U. Rafique, R. P. Davies, *Microporous Mesoporous Mater.* **2016**, *221*, 238-244; d) A. A. Alqadami, M. A. Khan, M. R. Siddiqui, Z. A. Alothman, *Microporous Mesoporous Mater.* **2018**, *261*, 198–206.
- [13] a) N. D. Rudd, H. Wang, E. M. A. Fuentes-Fernandez, S. J. Teat, F. Chen, G. Hall, Y. J. Chabal, J. Li, *ACS Appl. Mater. Interfaces* **2016**, *8*, 30294–30303; b) L. Esrafilii, V. Safarifarid, E. Tahmasebi, M. D. Esrafilii, A. Morsali, *New J. Chem.* **2018**, *42*, 8864-8873; c) C. Yu, X. Han, Z. Shao, L. Liu, H. Hou, *Cryst. Growth Des.* **2018**, *18*, 1474–1482; d) C. Yu, Z. Shao, H. Hou, *Chem. Sci.* **2017**, *8*, 7611–7619.
- [14] a) N. H. Alsmail, M. Suyetin, Y. Yan, R. Cabot, C. P. Krap, J. Lü, T. L. Easun, E. Bichoutskaia, W. Lewis, A. J. Blake, M. Schröder, *Chem. Eur. J.* **2014**, *20*, 7317 – 7324; b) B. T. Nguyen, H. L. Nguyen, T. C. Nguyen, K. E. Cordova, H. Furukawa, *Chem. Mater.* **2016**, *28*, 6243–6249.
- [15] T. Hu, H. Wang, B. Li, R. Krishna, H. Wu, W. Zhou, Y. Zhao, Y. Han, X. Wang, W. Zhu, Z. Yao, S. Xiang, B. Chen, *Nat. Commun.* **2015**, *6*, 7328.
- [16] S. Yao, J. Zhang, D. Shen, R. Xiao, S. Gu, M. Zhao, J. Liang, *J. Colloid Interface Sci.*, **2016**, *463*, 118-127.
- [17] a) J. Wang, W. Zhang, X. Yue, Q. Yang, F. Liu, Y. Wang, D. Zhang, Z. Li, J. Wang, *J. Mater. Chem. A* **2016**, *4*, 3893–3900; b) F. Li, X. Wang, T. Yuan, R. Sun, *J. Mater. Chem. A* **2016**, *4*, 11888–11896.
- [18] a) I. Langmuir, *J. Am. Chem. Soc.* **1918**, *40*, 1361–1403; b) F. S. Awad, K. M. AbouZeid, W. M. Abou El-Maaty, A. M. El-Wakil, M. S. El-Shall, *ACS Appl. Mater. Interfaces* **2017**, *9*, 34230–34242.
- [19] Y. Wang, D. Wu, Q. Wei, D. Wei, T. Yan, L. Yan, L. Hu, B. Du, *Sci. Rep.* **2017**, *7*, 10264.
- [20] a) L. Mi, H. Hou, Z. Song, H. Han, Y. Fan, *Chem. Eur. J.* **2008**, *14*, 1814. b) Z. Shao, C. Huang, J. Dang, Q. Wu, Y. Liu, J. Ding, H. Hou, *Chem. Mater.* **2018**, *30*, 7979. c) Z. Shao, C. Huang, Q. Wu, Y. Zhao, W. Xu, Y. Liu, J. Dang, H. Hou, *J. Hazard. Mater.*, **2019**, *378*, 120719.
- [21] J. S. Ogden, M. J. Ricks, *J. Chem. Phys.* **1972**, *56*, 1658-1662.
- [22] Y. Peng, H. Huang, Y. Zhang, C. Kang, S. Chen, L. Song, D. Liu, C. Zhong, *Nat. Commun.* **2018**, *9*, 187.
- [23] a) L. Wang, X. Zhao, J. Zhang, Z. Xiong, *Environ. Sci. Pollut. Res.* **2017**, *24*, 14198–14206. b) L. Zhang, Y. H. Hu, *J. Phys. Chem. C* **2011**, *115*, 7967–7971. c) M. Lalonde, W. Bury, O. Karagiari, Z. Brown, J. T. Hupp, O. K. Farha, *J. Mater. Chem. A*, **2013**, *1*, 5453.
- [24] D. Chen, W. Shen, S. Wu, C. Chen, X. Luo, L. Guo, *Nanoscale* **2016**, *8*, 7172-7179.
- [25] A. Jamali, A.A. Tehrani, F. Shemirani, A. Morsali, *Dalton Trans.* **2016**, *45*, 9193–9200.
- [26] X. Luo, L. Ding, J. Luo, *J. Chem. Eng. Data* **2015**, *60*, 1732-1743.
- [27] F. Rouhani, A. Morsali, *Chem. Eur. J.* **2018**, *24*, 5529-5537.
- [28] J. M. Rivera, S. Rincon, C. Ben Youssef, A. Zepeda, *J. Nanomater.* **2016**, *2016*, 9.
- [29] Q. Qin, Q. Wang, D. Fu, J. Ma, *Chem. Eng. J.* **2011**, *172*, 68–74.

FULL PAPER

FULL PAPER



F. Afshari Azar, A. Morsali*, J. Wang, P. C.

Junk

Page No. - Page No.

Title: Highest and Fastest Removal Rate of Pb(II) Ions through Rational Functionalized Decoration of MOF Cavity

TMU-56, exhibits high performance in removal of toxic Pb(II) metal ions from aqueous solutions. The existence of abundant strong chelating sites, along with large enough pore size lead not only to the highest uptake capacity for Pb(II) ions of 1130 mg g^{-1} , but also the fastest removal rate that has ever been reported for functionalized MOFs, which occurred in just 20 sec.